

# $H_2$ optimal actuator and sensor placement in the linearised complex Ginzburg–Landau system

By KEVIN K. CHEN<sup>†</sup> AND CLARENCE W. ROWLEY

Department of Mechanical and Aerospace Engineering, Princeton University, Princeton, NJ 08544, USA

(Received 12 January 2011)

The linearised complex Ginzburg–Landau equation is a model for the evolution of small fluid perturbations, such as in a bluff body wake. By implementing actuators and sensors and designing an  $H_2$  optimal controller, we control a supercritical, infinite-domain formulation of this system. We seek the optimal actuator and sensor placement that minimises the  $H_2$  norm of the controlled system, from flow disturbances to a cost on the perturbation and input magnitudes. We formulate the gradient of the  $H_2$  squared norm with respect to actuator and sensor placements, and iterate toward the optimal placement. When stochastic flow disturbances are present everywhere in the spatial domain, it is optimal to place the actuator just upstream of the origin and the sensor just downstream. With pairs of actuators and sensors, it is optimal to place each actuator slightly upstream of each corresponding sensor, and scatter the pairs throughout the spatial domain. When disturbances are only introduced upstream, the optimal placement shifts upstream as well. Global mode and Gramian analyses fail to predict the optimal placement; they produce  $H_2$  norms about five times higher than at the true optimum. The wavemaker region is a better guess for the optimal placement.

---

## 1. Introduction

Stability theory has been an active field of fluid mechanics research because of its prevalence in physical phenomena. A common characteristic of stability theory is the simplification of the full Navier–Stokes equations to an amplitude equation of reduced dimension. This is often done out of practicality, since reduced-dimensional models are more tractable and easier to analyse. The Ginzburg–Landau equation is one such model that is often used to study fluid instabilities in spatially developing flows (Williamson 1996); it has been applied to bluff body wakes, jets, and other configurations (see Chomaz *et al.* 1988; Cossu & Chomaz 1997; Lauga & Bewley 2004; Bagheri *et al.* 2009).

The Ginzburg–Landau equation describes the temporal and spatial evolution of velocity perturbations in a given flow configuration. It is a complex partial differential equation first-order in time and second-order in one spatial dimension, the streamwise direction. As such, it serves as a convenient starting point for establishing a flow control model without the complexities of a full two- or three-dimensional Navier–Stokes system. If flow field perturbations from a steady solution are sufficiently small, then the equation’s cubic term can be truncated to simplify the Ginzburg–Landau equation to a linear partial differential equation.

<sup>†</sup> Email address for correspondence: [kkchen@princeton.edu](mailto:kkchen@princeton.edu)

The articles by Bagheri *et al.* (2009) and Lauga & Bewley (2004) employed a flow control framework for the linearised Ginzburg–Landau equation. They modeled the flow dynamics, actuator effect, and probe sensing as a standard linear state space. This representation carries the benefit that linear time-invariant (LTI) control theory is a highly developed field of study; results from optimal control, robust control, and model reduction theories are directly applicable. These papers analysed the transient and long-time stability of the Ginzburg–Landau system using a single-input, single-output (SISO) feedback loop—that is, with one actuator manipulating the flow at one point in space, acting on information from one sensor located at another point in space. Bagheri *et al.* emphasised model reduction of the system and linear quadratic Gaussian (LQG) control (which is a specific instance of  $H_2$  optimal control) in the presence of an upstream disturbance. Lauga & Bewley, on the other hand, focused on  $H_\infty$ -based robust control.

The present study expands on the  $H_2$  optimal control framework by investigating where actuators and sensors should be placed for maximum reduction of the flow perturbation and actuator effort, given an exogenous flow disturbance. There does not currently exist an analytically rigorous study on optimal actuator and sensor placement for fluid systems. Bagheri *et al.* (2009) and Åkervik *et al.* (2007) stated that sensor locations should overlap with unstable global modes, and actuator locations with corresponding adjoint modes; they placed their sensor and actuator at the mode magnitude maxima. The detectability and stabilisability conditions are necessary for the construction of the  $H_2$  optimal control solution (Doyle *et al.* 1989). As will become evident in this paper, however, actuator and sensor placement by modal analysis yields suboptimal control. Although such a placement may be sufficient for preventing large-scale self-sustaining global oscillations, it may be insufficient for applications where transient growth needs to be reduced.

Gillies (2000) placed an actuator in the absolutely unstable part of the domain, and experimentally showed that his controllers were successful only when the sensors were also in the absolutely unstable domain. These results were consistent with those of Rousopoulos (1993), who experimented with sensor placement in a wind tunnel and a water channel. Cohen *et al.* (2004) simulated the Navier–Stokes equations in two dimensions and placed sensors where proper orthogonal decomposition modes had energy extrema. Lauga & Bewley (2004) placed an actuator and a sensor in the wavemaker region of the Ginzburg–Landau equation.

Much of the analytically rigorous literature on optimal actuator and sensor placement is related to the vibration control of flexible structures. For instance, Moheimani & Ryall (1999) placed collocated actuator and sensor pairs where they were able to control all important vibration modes. Kondoh, Yatomi & Inoue (1990) employed Powell’s method of multidimensional function minimisation to locate  $H_2$  optimal actuator and sensor positions, but reported that the iterative technique became difficult as the number of actuators and sensors increased. Hiramoto, Doki & Obinata (2000) formulated the gradient of the controlled system’s  $H_2$  norm with respect to actuator and sensor locations, allowing the use of gradient-based minimisation techniques. The framework developed, however, assumed collocation of the actuator and sensor.

Vibration control of flexible structures benefits from the fact that the dynamical evolution operator is normal (Hiramoto *et al.* 2000), and eigenfunctions are orthogonal (Halim & Moheimani 2003). On the other hand, the linearised Ginzburg–Landau and Navier–Stokes operators are non-normal, and their global modes do not form an orthogonal basis (Bagheri *et al.* 2009; Cossu & Chomaz 1997). Therefore, methods for optimal placement in the flexible structures literature generally do not apply to fluid systems. Ideally, techniques should analytically or numerically compute optimal placement without iteration. In the absence of such techniques, the Powell’s method of Kondoh *et al.* (1990) and the

gradient-based minimisation of Hiramoto *et al.* (2000) serve as good starting points for the Ginzburg–Landau system.

In this paper, we seek the actuator and sensor placement that minimises the perturbation magnitude and actuator effort of the Ginzburg–Landau system in an  $H_2$  sense. We investigate cases in which a white noise flow disturbance is present everywhere in the domain, or only in the upstream region. The underlying idea is that while  $H_2$  optimal control theory can provide the “best” controller given an actuator and sensor placement, the “best” placement should ideally be sought in conjunction. We develop an improved formulation of Hiramoto *et al.*’s  $H_2$  norm gradient. We employ the conjugate gradient method of multidimensional function minimisation for SISO as well as multiple-input, multiple-output (MIMO) control of the Ginzburg–Landau equation. For the SISO cases, we compare the conjugate gradient results to brute force sampling results, where we evaluate the  $H_2$  optimal controller and the corresponding system norm for a large test matrix of actuator and sensor positions. Finally, we discuss the failure of global mode and Gramian analyses in yielding optimal placement, and we suggest that the wavemaker region is a better indicator of the optimal placement.

## 2. Complex Ginzburg–Landau equation

### 2.1. Continuous representation

A complete discussion of the Ginzburg–Landau equation is too expansive to be given here. For a more comprehensive review, refer to the review article by Bagheri *et al.* (2009).

For a velocity or streamfunction perturbation amplitude given by the real part of  $q(x, t)$ , the complex Ginzburg–Landau equation is

$$\frac{\partial q}{\partial t} + \nu \frac{\partial q}{\partial x} = \mu(x) q + \gamma \frac{\partial^2 q}{\partial x^2} - a |q|^2 q. \quad (2.1)$$

We choose the spatial domain of  $q$  to be fully infinite, requiring  $q(\pm\infty, t) = 0$  (Cossu & Chomaz 1997; Chomaz 2005). This allows perturbations to grow and decay throughout the entire streamwise dimension. With this choice of a domain, we typically assume that the physical feature of interest is at  $x = 0$ . The complex advection speed is  $\nu = U + 2ic_u$ , the complex diffusion parameter is  $\gamma = 1 + ic_d$ , and the amplification factor is  $\mu(x) = \mu_0 - c_u^2 + \mu_2 x^2/2$  (Bagheri *et al.* 2009). The mean advection velocity is given by  $U > 0$ , and  $c_u$ ,  $\mu_0$ , and  $a$  are also positive quantities;  $\mu_2$  and  $c_d$  are negative (Cossu & Chomaz 1997; Chomaz 2005). Numerical values of these parameters are determined empirically (Williamson 1996; Roussopoulos & Monkewitz 1996).

The nonlinear term  $-a |q|^2 q$  causes a Hopf bifurcation expected in many geometrical configurations, for instance, as in Sreenivasan, Strykowski & Olinger (1987). In a linear analysis, the flow is assumed to be near the equilibrium state  $q = 0$ ; thus,  $-a |q|^2 q \approx 0$ . The resulting linear equation is

$$\dot{q} = Lq, \quad (2.2a)$$

where

$$L \triangleq -\nu \frac{\partial}{\partial x} + \mu(x) + \gamma \frac{\partial^2}{\partial x^2} \quad (2.2b)$$

defines the linear operator  $L$ . From this point forward, we will always truncate the cubic term and refer only to the linear system.

We now comment on the stability properties of the linearised Ginzburg–Landau system, drawing from results found in Bagheri *et al.* (2009) and Cossu & Chomaz (1997). In the

parabolic construction  $\mu(x) = (\mu_0 - c_u^2) + \mu_2 x^2/2$ , the region of amplification is the part of the domain where  $\mu(x) > 0$ ; this corresponds to  $-\sqrt{-2(\mu_0 - c_u^2)/\mu_2} < x < \sqrt{-2(\mu_0 - c_u^2)/\mu_2}$ . The quantity  $\mu_0 - c_u^2$  is the greatest amplification factor present in the physical domain, occurring at  $x = 0$ ;  $\mu_0$  is derived from the Reynolds number. If  $\mu_0 - c_u^2 < 0$ , then the flow is stable everywhere, and all perturbations decay with time. Otherwise, at least some part of the domain exhibits amplification (convective or absolute instability), and  $c_u$  is the most unstable spatial wavenumber.

In the analysis of parallel flows (where  $\mu$  is constant), we construct a transitional value  $\mu_t = U_{max}^2 / (4|\gamma|^2)$ , with  $U_{max} = U + 2c_d c_u$  the group velocity. When  $0 < \mu < \mu_t$ , the domain is convectively unstable. Perturbations may grow in time, but ultimately sweep downstream; the amplitude at any fixed location eventually decays to zero. When  $\mu_t < \mu$ , the domain is absolutely unstable, and all perturbations blow up to complex infinity.

Returning to the non-parallel case, where  $\mu$  is parabolic in space, we also define a critical value  $\mu_c = \mu_t + |h| \cos((\text{Arg } \gamma)/2)/2$ , where  $h = \sqrt{-2\mu_2\gamma}$ . Global stability is lost if and only if  $\mu_0 > \mu_c$ ; this is a direct result of the eigen decomposition of L. Eigenvalues, eigenmodes, and adjoint modes are given respectively by

$$\lambda_n = \mu_0 - c_u^2 - \frac{\nu^2}{4\gamma} - \left(n + \frac{1}{2}\right) h \quad (2.3a)$$

$$\phi_n(x) = \exp\left(\frac{1}{2}\left(\frac{\nu x}{\gamma} - \chi^2 x^2\right)\right) H_n(\chi x) \quad (2.3b)$$

$$\psi_n(x) = \exp\left(-\frac{\bar{\nu}}{\bar{\gamma}}x\right) \bar{\phi}_n(x), \quad (2.3c)$$

where  $n = 0, 1, \dots$ ,  $\chi = (-\mu_2/(2\gamma))^{1/4}$ ,  $H_n$  is the  $n^{\text{th}}$  Hermite polynomial, and  $\bar{(\cdot)}$  indicates a complex conjugate. If  $\text{Re}[\lambda_0] > 0$ , then the system must be globally unstable. Otherwise, it is globally stable and perturbations eventually decay with time, but transient perturbation growth may still exist.

Finally, we note briefly that  $\mu_2$  denotes how non-parallel the flow is; it is partly responsible for determining the size of the amplification region. In addition,  $c_d$  is a dispersion parameter, but we will not discuss it further. See Bagheri *et al.* (2009) for additional details.

The Ginzburg–Landau parameters chosen for this study are drawn from Bagheri *et al.* (2009) and are shown in table 1. This study primarily investigates a supercritical, globally unstable system, with  $\mu_0 = 1.03\mu_c$ . When we consider subcritical, globally stable systems, however, we use  $\mu_0 = 0.96\mu_c$ . We always assume supercriticality unless stated otherwise.

## 2.2. Discrete representation

To model the Ginzburg–Landau equation as an LTI state space, we spatially discretise the physical domain. We create a domain discretisation and a spectral formulation of  $\partial/\partial x$  and  $\partial^2/\partial x^2$  using weighted Hermite polynomials, as in Bagheri *et al.* (2009). We draw the discretisation and associated differentiation operators from Weideman & Reddy (2000). The physical domain is represented using  $N = 100$  grid points, and these points  $\{x_1, x_2, \dots, x_N\}$  are the roots of  $H_N(\chi x)$ . With this choice of  $N$ , the discretised domain stretches from  $x_1 = -56.06$  to  $x_N = 56.06$ . For the globally unstable system studied, the region of amplification is  $-8.60 < x < 8.60$ . We choose  $N = 100$  because it achieves sufficient accuracy while maintaining problem tractability. To check for convergence of results in  $N$ , we test systems with one actuator and one sensor, and with two actuators and two sensors. In both cases, we introduce flow disturbances across the entire spatial

variable	description	value
$U$	mean advection velocity	2.0
$c_u$	most unstable wavenumber	0.2
$c_d$	dispersion parameter	-1.0
$\mu_0$	overall amplification	0.41 (0.38)
$\mu_2$	degree of non-parallelism	-0.01
$\mu_t$	transitional $\mu$	0.32
$\mu_c$	critical $\mu$	0.40
$a$	nonlinearity	not used
$x_1, x_N$	extent of discretised domain	-56.06, 56.06
$\pm\sqrt{-2(\mu_0 - c_u^2)/\mu_2}$	extent of region of amplification	$\pm 8.60$ ( $\pm 8.25$ )
$x_d$	upstream disturbance location	-11.0
$\sigma$	Gaussian width	0.4

TABLE 1. Ginzburg–Landau parameters. Subcritical parameters are shown in parentheses.

domain (see §3.1 for details). Increasing  $N$  from 100 to 200 changes the computed optimal actuator and sensor placement by less than 1.0% of the amplification region’s length.

Using this discretisation scheme, we construct the state vector  $\mathbf{q} = [q_1 \ \cdots \ q_N]^T$ , where  $q_j = q(x_j)$  for  $j = 1, 2, \dots, N$ . Let  $D$  be the Hermite spectral derivative operator, and  $\Delta$  be the corresponding second derivative operator. Also, let  $\boldsymbol{\mu}$  be  $\mu(x)$  discretised in the same way as  $\mathbf{q}$ . Then the discrete representation of the linearised Ginzburg–Landau equation is

$$\dot{\mathbf{q}} = A\mathbf{q}, \tag{2.4a}$$

where

$$A \triangleq -\nu D + \text{diag}(\boldsymbol{\mu}) + \gamma \Delta \tag{2.4b}$$

is the discrete linearised Ginzburg–Landau operator.

### 3. $H_2$ optimal control and placement

#### 3.1. State space setup

Let us return momentarily to the continuous-space linearised Ginzburg–Landau equation. Instead of implementing a particular type of flow actuator or sensing probe, we apply generic actuation and sensing drawn from the standard state space setup. This way, we can easily take advantage of available LTI tools. We also insert a white noise disturbance  $d$ , which may be present everywhere in the spatial domain, or centred in the upstream domain. Assume a small sensor white noise  $n$ . For a single actuator located at  $x = x_a$  and a single sensor at  $x = x_s$ , the state space is

$$\frac{\partial q}{\partial t}(x, t) = Lq(x, t) + \exp\left(-\frac{(x - x_a)^2}{2\sigma^2}\right) u(t) + d(x, t) \tag{3.1a}$$

$$y(t) = \left\langle q(x, t), \exp\left(-\frac{(x - x_s)^2}{2\sigma^2}\right) \right\rangle + n(x, t), \tag{3.1b}$$

where  $\langle f_1, f_2 \rangle \triangleq \int_{-\infty}^{\infty} \bar{f}_2 f_1 dx$  is an inner product. The state  $q$ , input signal  $u$ , output signal  $y$ , disturbance  $d$ , and noise  $n$  are all complex, and we choose  $\sigma = 0.4$ .

In discretised form, with  $\mathbf{A}$  given by (2.4b) and all other variables explained below, we recover the standard state space

$$\dot{\mathbf{q}} = \mathbf{A}\mathbf{q} + \mathbf{B}_2\mathbf{u} + W^{\frac{1}{2}}\mathbf{d} \quad (3.2a)$$

$$\mathbf{y} = \mathbf{C}_2\mathbf{q} + V^{\frac{1}{2}}\mathbf{n}. \quad (3.2b)$$

In SISO control,  $\mathbf{u}$  and  $\mathbf{y}$  are complex scalars, and  $\mathbf{B}_2$  is an  $N$ -by-1 vector discretising  $\exp\left(-\frac{(x-x_a)^2}{2\sigma^2}\right)$ . For discretised sensing, note that a weighting matrix must be used to carry out the integration implied by (3.1b). Let

$$\mathbf{M} = \frac{1}{2}\text{diag}\left([x_2 - x_1 \quad x_3 - x_1 \quad \cdots \quad x_{i+1} - x_{i-1} \quad \cdots \quad x_m - x_{m-2} \quad x_m - x_{m-1}]\right) \quad (3.3)$$

be the weighting matrix corresponding to the trapezoidal integration operator, and let  $\mathbf{s}$  be the  $n$ -by-1 discretisation of  $\exp\left(-\frac{(x-x_s)^2}{2\sigma^2}\right)$ . Then the inner product in (3.1b) transforms to  $\langle \mathbf{q}, \mathbf{s} \rangle$ , where  $\langle \mathbf{v}_1, \mathbf{v}_2 \rangle = \mathbf{v}_2^* \mathbf{M} \mathbf{v}_1$  is the discrete inner product and  $(\cdot)^*$  indicates a conjugate transpose. This yields  $\mathbf{C}_2 = \mathbf{s}^T \mathbf{M}$ . In the case of MIMO control, suppose that there exist  $m_a$  actuators and  $m_s$  sensors. Let  $\mathbf{b}^j$  be the discretisation of the  $j$ th actuator, and  $\mathbf{s}^k$  the  $k$ th sensor. Then  $\mathbf{B}_2 = [\mathbf{b}^1 \quad \cdots \quad \mathbf{b}^{m_a}]$ , and  $\mathbf{C}_2 = [\mathbf{s}^1 \quad \cdots \quad \mathbf{s}^{m_s}]^T \mathbf{M}$ .

The disturbance and sensor noise are complex white noise stochastic processes. In the case of a disturbance pervading the entire domain,  $\mathbf{d}$  is an  $N$ -by-1 complex white noise signal with covariance  $E(\mathbf{d}\mathbf{d}^*) = I$  (and  $E$  the expected value), and we choose  $W^{\frac{1}{2}} = I$ . If the disturbance is upstream, then  $\mathbf{d}$  is a complex white noise scalar with unit covariance, and  $W^{\frac{1}{2}}$  is the  $N$ -by-1 vector discretisation of  $\exp\left(-\frac{(x-x_d)^2}{2\sigma^2}\right)$ ;  $x_d$  is fixed at  $-11.0$ . We do not wish to place any particular focus on sensor noise in this study, but the noise must be present for the LQG formulation to be well-posed. Therefore,  $\mathbf{n}$  is an  $m_s$ -by-1 complex white noise signal with covariance  $E(\mathbf{n}\mathbf{n}^*) = I$ , and we choose  $V^{\frac{1}{2}} = 2 \cdot 10^{-4}I$  so that the sensor noise is present but minimal. It will be apparent later that the LQG controller remains well-behaved for this small choice of  $V^{\frac{1}{2}}$ .

### 3.2. Linear quadratic Gaussian framework

Having set up the governing dynamics and input/output relations in (3.1–3.2), we now design a controller that determines the control signal  $u(t)$  from the sensor output  $y(t)$ . In particular, we seek the relation from  $y$  to  $u$  that minimises the perturbation magnitude  $\int_{-\infty}^{\infty} |q(x, t)|^2 dx$ . This minimisation is the ultimate goal of Ginzburg–Landau control. Realistically, however, we must also keep the input size  $|u(t)|^2$  within bounds; a very large input size may be non-physical. Therefore, we establish a cost function

$$J = \beta^2 \int_{-\infty}^{\infty} |q(x, t)|^2 dx + |u(t)|^2 \quad (3.4)$$

to minimise using the right choice of a controller. The positive scalar  $\beta$  controls the balance between maintaining a small perturbation size and maintaining a small input size. In this study, we choose  $\beta = 7$ . We discuss different choices of  $\beta$  in §4.2.

In discrete space, the cost function takes the form  $J = \mathbf{q}^* \mathbf{Q} \mathbf{q} + \mathbf{u}^* \mathbf{R} \mathbf{u}$ , where  $\mathbf{Q}$  and  $\mathbf{R}$  are user-specified penalties on the state and inputs sizes. To be consistent with (3.4), we use  $\mathbf{Q} = \beta^2 \mathbf{M}$  and  $\mathbf{R} = I$ . In vector form, the cost on the perturbation and input sizes are given by  $\mathbf{J}_1 = \mathbf{Q}^{\frac{1}{2}} \mathbf{q}$  and  $\mathbf{J}_2 = \mathbf{R}^{\frac{1}{2}} \mathbf{u}$ , where the matrix square root  $Z^{\frac{1}{2}}$  satisfies  $(Z^{\frac{1}{2}})^* Z^{\frac{1}{2}} \equiv Z$ . Since the disturbance  $\mathbf{d}$  and sensor noise  $\mathbf{n}$  are exogenous inputs, minimising  $J$  is equivalent to minimising the gain from  $\mathbf{d}$  and  $\mathbf{n}$  to the cost vectors  $\mathbf{J}_1$  and  $\mathbf{J}_2$ . To

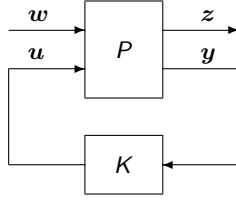


FIGURE 1. General control problem formulation  $G$ .

establish the relation from  $\mathbf{d}$  and  $\mathbf{n}$  to  $\mathbf{J}_1$  and  $\mathbf{J}_2$ , we first incorporate the cost vectors into the state space in (3.2) to yield

$$P : \begin{bmatrix} \dot{\hat{\mathbf{q}}} \\ \mathbf{z} \\ \mathbf{y} \end{bmatrix} = \begin{bmatrix} A & B_1 & B_2 \\ C_1 & 0 & D_{12} \\ C_2 & D_{21} & 0 \end{bmatrix} \begin{bmatrix} \hat{\mathbf{q}} \\ \mathbf{w} \\ \mathbf{u} \end{bmatrix}, \quad (3.5a)$$

where

$$\mathbf{z} = \begin{bmatrix} \mathbf{J}_1 \\ \mathbf{J}_2 \end{bmatrix} \quad \mathbf{w} = \begin{bmatrix} \mathbf{d} \\ \mathbf{n} \end{bmatrix} \quad (3.5b,c)$$

and

$$B_1 = [W^{\frac{1}{2}} \quad 0] \quad C_1 = \begin{bmatrix} Q^{\frac{1}{2}} \\ 0 \end{bmatrix} \quad D_{12} = \begin{bmatrix} 0 \\ R^{\frac{1}{2}} \end{bmatrix} \quad D_{21} = [0 \quad V^{\frac{1}{2}}]. \quad (3.5d-g)$$

Equation (3.5a) is called the “plant” or simply  $P$ . Figure 1 is a pictorial representation of the control problem. The controller  $K$  determines the input signal  $\mathbf{u}$  based on the sensor output  $\mathbf{y}$ . The external input to the system is the flow disturbance and sensor noise in  $\mathbf{w}$ , and the system output is the cost  $\mathbf{z}$  to be minimised.

In the construction of the general LTI controller, we choose matrices  $K_A$ ,  $K_B$ ,  $K_C$ , and  $K_D$  such that

$$K : \begin{bmatrix} \dot{\hat{\mathbf{q}}} \\ \mathbf{u} \end{bmatrix} = \begin{bmatrix} K_A & K_B \\ K_C & K_D \end{bmatrix} \begin{bmatrix} \hat{\mathbf{q}} \\ \mathbf{y} \end{bmatrix} \quad (3.6)$$

determines the actuation signal  $\mathbf{u}$  based on the output signal  $\mathbf{y}$ . The variable  $\hat{\mathbf{q}}$  is the state of the controller, and is typically an estimate of the plant state  $\mathbf{q}$ . The LQG controller is the LTI controller that minimises the  $H_2$  norm of the transfer function from  $\mathbf{d}$  and  $\mathbf{n}$  to  $\mathbf{J}_1$  and  $\mathbf{J}_2$ . Suppose that  $G(s)$  is that matrix transfer function. In other words, for  $s \in \mathbb{C}$  and disturbance and sensor noise inputs of the form  $e^{st}$ ,

$$\begin{bmatrix} \mathbf{J}_1 \\ \mathbf{J}_2 \end{bmatrix} = G(s) \begin{bmatrix} \mathbf{d} \\ \mathbf{n} \end{bmatrix} \quad (3.7)$$

dictates the gain and phase from  $\mathbf{d}$  and  $\mathbf{n}$  to  $\mathbf{J}_1$  and  $\mathbf{J}_2$ . Then the  $H_2$  norm is defined as

$$\gamma_2 \triangleq \|G\|_2 \triangleq \sqrt{\frac{1}{2\pi} \int_{-\infty}^{\infty} \text{tr}(G^*(i\omega) G(i\omega)) \, d\omega} \quad (3.8)$$

and is an average (instead of a worst-case) measure of the gain provided by  $G$ . Thus, given exogenous inputs, minimising the perturbation magnitude and actuator effort is equivalent to minimising  $\|G\|_2$ . We implement the LQG controller so that  $\|G\|_2$  is automatically minimised.

To construct the LQG controller, solve the continuous algebraic Riccati equations

$$A^*X + XA - XB_2R^{-1}B_2^*X + C_1^*C_1 = 0 \quad (3.9a)$$

$$AY + YA^* - YC_2^*V^{-1}C_2Y + B_1B_1^* = 0 \quad (3.9b)$$

for  $X$  and  $Y$ , and set  $F = R^{-1}B_2^*X$  and  $L = YC_2^*V^{-1}$ . The LQG controller is then given by

$$K : \begin{bmatrix} \dot{\hat{q}} \\ \mathbf{u} \end{bmatrix} = \begin{bmatrix} A - B_2F - LC_2 & L \\ -F & 0 \end{bmatrix} \begin{bmatrix} \hat{q} \\ \mathbf{y} \end{bmatrix}. \quad (3.10)$$

The plant (3.5a) and LQG controller (3.10) can be combined to form a single system, known as the linear fractional transformation (LFT) of  $G$  and  $K$ . One representation of the LFT is

$$\begin{bmatrix} \dot{\hat{q}} \\ \dot{\hat{q}} \\ \mathbf{z} \end{bmatrix} = \begin{bmatrix} A & -B_2F & B_1 \\ LC_2 & A - B_2F - LC_2 & LD_{21} \\ C_1 & -D_{12}F & 0 \end{bmatrix} \begin{bmatrix} \mathbf{q} \\ \hat{q} \\ \mathbf{w} \end{bmatrix}. \quad (3.11)$$

(Often, the LFT is expressed using an error  $\mathbf{e} = \hat{\mathbf{q}} - \mathbf{q}$  instead of directly using the state estimate  $\hat{\mathbf{q}}$ .) Denote the upper-left two-by-two matrix block by  $Z_A$ , the upper-right two-by-one block by  $Z_B$ , and the lower-left one-by-two block by  $Z_C$ . If we compute Gramians  $W_c$  and  $W_o$  by the Lyapunov equations

$$Z_A W_c + W_c Z_A^* + Z_B Z_B^* = 0 \quad (3.12a)$$

$$Z_A^* W_o + W_o Z_A + Z_C^* Z_C = 0, \quad (3.12b)$$

then the LQG-controlled system's  $H_2$  squared norm is

$$\Gamma_2 \triangleq \|\mathbf{G}\|_2^2 = \text{tr}(Z_C W_c Z_C^*) \quad (3.13a)$$

$$= \text{tr}(Z_B^* W_o Z_B). \quad (3.13b)$$

The above formulations, however, require solutions of  $2N$ -by- $2N$  matrix equations. A simpler  $N$ -by- $N$  formulation is given by

$$\Gamma_2 = \text{tr}(C_1 Y C_1^*) + \text{tr}(V^{-1} C_2 Y X Y C_2^*) \quad (3.14a)$$

$$= \text{tr}(B_1^* X B_1) + \text{tr}(R^{-1} B_2^* X Y X B_2). \quad (3.14b)$$

For a more thorough study of  $H_2$  optimal control and the LQG, consult Doyle *et al.* (1989) and Skogestad & Postlethwaite (2005).

### 3.3. Perturbation technique for optimal placement

Suppose that a choice of  $B_2$  and  $C_2$  is  $H_2$  optimal. That is, the choice of  $B_2$  and  $C_2$  provides the best-performing  $H_2$  optimal controller, given matrix constraints described in §3.1. It is necessary, but not sufficient, for an appropriately constrained perturbation  $\delta B_2 \neq 0$  to produce  $\delta \Gamma_2 = 0$ ; similarly,  $\delta C_2 \neq 0$  must produce  $\delta \Gamma_2 = 0$ . The constraint on  $\delta B_2$  is that it must equal the change in  $B_2$  when an actuator position moves from  $x_a$  to  $x_a + \delta x_a$ , for a small  $\delta x_a$ . If there is multiple actuation, then  $\delta B_2$  can be a perturbation along any one of the actuator positions. The constraint on  $\delta C_2$  is completely analogous, except that it is necessary to pay careful attention to the discretised integration operator  $M$ .

If the actuator location is perturbed from  $B_2$  to  $B_2 + \delta B_2$ , then we can define  $\delta X$  such that (3.9a) produces a perturbed solution  $X + \delta X$ . The exact representation is

$$A^*(X + \delta X) + (X + \delta X)A - (X + \delta X)(B_2 + \delta B_2)R^{-1}(B_2 + \delta B_2)^*(X + \delta X) + C_1^*C_1 = 0. \quad (3.15)$$

The  $O(\delta^0)$  component returns (3.9a), as expected. The  $O(\delta^1)$  component is

$$(A - B_2 R^{-1} B_2^* X)^* \delta X + \delta X (A - B_2 R^{-1} B_2^* X) - X (\delta B_2 R^{-1} B_2^* + B_2 R^{-1} \delta B_2^*) X = 0, \quad (3.16)$$

which is a Lyapunov equation for  $\delta X$ . The perturbation in  $X$  then produces  $\delta\Gamma_2 = \text{tr}(V^{-1} C_2 Y \delta X Y C_2^*)$  from (3.14a). At the optimal actuator location,

$$\delta\Gamma_2 = \text{tr}(V^{-1} C_2 Y \delta X Y C_2^*) = 0. \quad (3.17)$$

In summary, given an appropriately constrained  $B_2$  and  $\delta B_2$ , the  $H_2$  optimal  $B_2$  is one that produces  $\text{tr}(V^{-1} C_2 Y \delta X Y C_2^*) = 0$ , where  $\delta X$  is the solution to (3.16) and  $X$  is the solution to (3.9a). For this choice of  $B_2$ , the actuator position and the controller are simultaneously optimised to minimise the magnitude of flow perturbations and actuator input. Additional steps are required, however, to ensure that the  $B_2$  satisfying  $\delta\Gamma_2 = 0$  actually minimises  $\Gamma_2$ , instead of yielding a maximum or saddle point.

The procedure for finding the optimal sensor location is similar to the previously described steps. For an appropriate choice of  $C_2$  and  $\delta C_2$ , the optimal  $C_2$  is the one that first yields  $Y$  by (3.9b), then yields  $\delta Y$  by the Lyapunov equation

$$(A - Y C_2^* V^{-1} C_2) \delta Y + \delta Y (A - Y C_2^* V^{-1} C_2)^* - Y (\delta C_2^* V^{-1} C_2 + C_2^* V^{-1} \delta C_2) Y = 0, \quad (3.18)$$

and finally satisfies

$$\delta\Gamma_2 = \text{tr}(R^{-1} B_2^* X \delta Y X B_2) = 0. \quad (3.19)$$

Since the Riccati equations in (3.9) must typically be solved numerically, we do not propose an analytical procedure for finding actuator and sensor placements yielding  $\delta\Gamma_2 = 0$ . Instead, we now create a framework where a gradient-based function minimisation can be used to iterate toward the optimal placements. For a set of actuator positions  $\{x_a^1, \dots, x_a^{m_a}\}$  and sensor positions  $\{x_s^1, \dots, x_s^{m_s}\}$ ,  $\Gamma_2$  is obtained by solving (3.9) and (3.14). For a perturbation of the  $j$ th actuator position  $x_a^j$  by an amount  $\delta x_a^j$ , solve (3.16) for  $\delta X^j$  and set

$$\frac{\delta\Gamma_2}{\delta x_a^j} = \frac{\text{tr}(V^{-1} C_2 Y \delta X^j Y C_2^*)}{\delta x_a^j}. \quad (3.20a)$$

For a perturbation of the  $k$ th sensor position  $x_s^k$  by an amount  $\delta x_s^k$ , solve (3.18) for  $\delta Y^k$  and set

$$\frac{\delta\Gamma_2}{\delta x_s^k} = \frac{\text{tr}(R^{-1} B_2^* X \delta Y^k X B_2)}{\delta x_s^k}. \quad (3.20b)$$

Note that the Riccati solutions  $X$  and  $Y$  are computed while solving for  $\Gamma_2$ , and can be reused while solving the Lyapunov equations needed for  $\nabla\Gamma_2$ . Thus, we solve two Riccati equations for every evaluation of  $\Gamma_2$ , and  $m_a + m_s$  Lyapunov equations for every evaluation of the  $(m_a + m_s)$ -by-1 vector  $\nabla\Gamma_2$ .

This technique for computing  $\nabla\Gamma_2$  is similar to the method proposed by Hiramoto *et al.* (2000), but is believed to be more computationally efficient. Because Hiramoto *et al.* computed  $\Gamma_2$  using the LFT of the controlled system, each component of  $\nabla\Gamma_2$  required the solution to a  $2N$ -by- $2N$  Lyapunov equation; see (3.11–3.13). On the other hand, the method we propose reduces this size to  $N$ -by- $N$ . Using the Lyapunov equation solvers selected for this study, our proposed method should provide a speedup by a factor of approximately six.

In this study, we employ a Polak-Ribière conjugate gradient method, using a modified Brent’s method of line minimisation that uses derivative information. Brent’s method

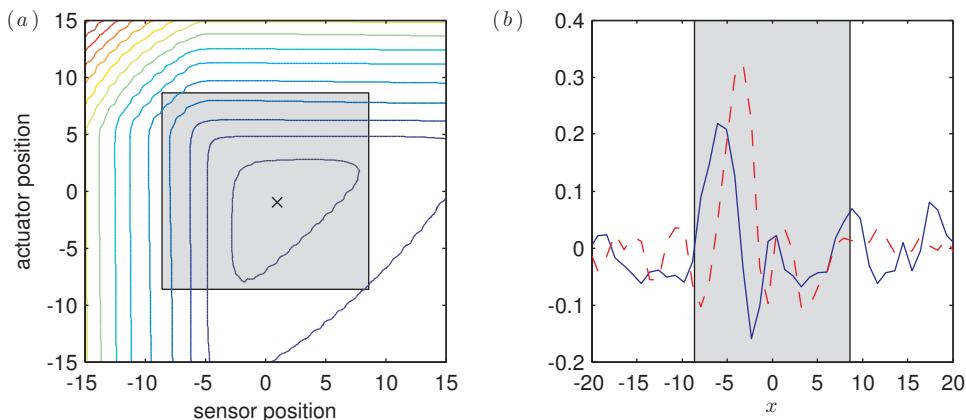


FIGURE 2. (a) Contours of  $\log_{10} \gamma_2$  and the optimal placement ( $\times$ ), with disturbances introduced everywhere. The innermost contour is  $\log_{10} \gamma_2 = 2$ , and each subsequent contour increments by 0.5. (b) A sample snapshot of the controlled perturbation  $q$ , shown as real (solid/blue) and imaginary (dashed/red) parts. The actuator is at  $x_a = -1.00$  and the sensor is at  $x_s = 1.00$ . In both plots, the region of amplification is shaded grey.

also requires a bracketing function that provides bounds on the line minimum. These methods are robust in the sense that they are unlikely to lose numerical stability, and they are generally efficient as well. Implementation details can be found in Press *et al.* (2007).

## 4. Results

### 4.1. Brute force sampling

To understand the effect of SISO actuator and sensor positions more fully, we first perform a brute force sampling of the LQG-controlled system's  $H_2$  norm. Instead of implementing a minimisation algorithm, we map out  $\gamma_2(x_a, x_s)$  over a test matrix spanning actuator and sensor positions in  $\{-15.00, -14.75, \dots, 15.00\}$ . The results for a white noise disturbance present across the entire spatial domain are plotted in figure 2(a). In Figure 2(b), we run a simulation of the LQG-controlled system and show a sample snapshot. Without control, the state would blow up in the region of amplification because the system would be globally unstable.

Some qualitative features are immediately obvious from figure 2(a). First, the optimal placement is approximately  $x_a = -1.00$  and  $x_s = 1.00$ , at which  $\gamma_2 = 46.1$ ; we will refine these numbers later through the use of iterative minimisation. Second, a penalty exists for placing the actuator too far downstream. This is an intuitive result—since the flow in question is convection-driven, a downstream actuator is able to influence less of the physical domain. Third, a similar penalty exists for placing the sensor too far upstream. Recall that the amplification factor  $\mu(x)$  is an inverted parabola with roots at  $\pm 8.60$ . If the sensor is too far upstream, then the detected disturbances naturally dampen before they reach the region of amplification. Thus, the disturbances amplified in this region would not primarily be the ones observed by the sensor. Finally, excessive time delay (positioning the sensor too far downstream of the actuator) has a detrimental effect on perturbation control. This is also a result of the convection-driven nature of the system. If the sensor is too far downstream of the actuator, then the information it receives will

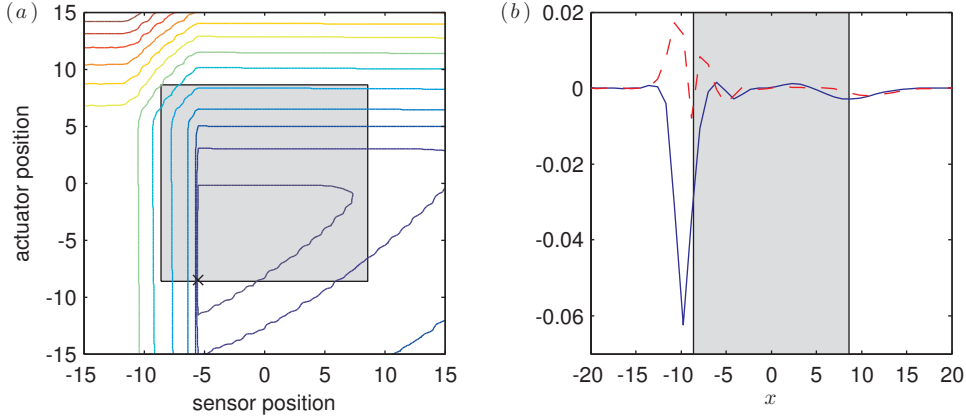


FIGURE 3. (a): Contours of  $\log_{10} \gamma_2$  and the optimal placement ( $\times$ ), for the case of an upstream disturbance introduced at  $x_d = -11.00$ . The innermost contour is  $\log_{10} \gamma_2 = 1.0$ , and each subsequent contour increments by 0.5. (b): A sample snapshot of the controlled perturbation  $q$ , shown as real (solid/blue) and imaginary (dashed/red) parts. The actuator is at  $x_a = -8.50$  and the sensor is at  $x_s = -5.50$ . In both plots, the region of amplification is shaded grey.

have already passed the actuator for some time. Thus, the actuator would be acting on outdated information, and the feedback would effectively result in a time lag.

Data for a flow disturbance introduced around  $x_d = -11.00$  are shown in figure 3(a), with a sample snapshot shown in figure 3(b). The qualitative features of this  $\gamma_2(x_a, x_s)$  map are similar to those of figure 2(a), but we highlight a few differences. First, the optimal placement is now approximately  $x_a = -8.50$  and  $x_s = -5.50$ , which is much further upstream than in the previous case. In the sample snapshot shown in figure 3(b), we note that the controller is extremely effective in reducing the perturbation magnitude within the region of amplification.

Intuitively, we might expect an optimal placement  $x_s \approx x_d$ , so that the sensor placement coincides with the disturbance source. Indeed, such a placement allows the state estimate  $\hat{q}$  to match the true state  $q$  very closely in the disturbance region. This placement, however, is far from optimal. As a result of the strong amplification downstream of the disturbance source, even the smallest estimator error  $e = \hat{q} - q$  in the disturbance region can amplify significantly. By placing the sensor downstream of the disturbance source, the estimator is better able to reduce the error  $e$  in the region of amplification, where accurate state estimation is critically important.

The second difference in the case of upstream disturbances is that the optimal placement is not robust. Although the optimal placement is unique, figure 3(a) shows that a small upstream shift in  $x_s$  drastically increases  $\gamma_2$ . The topology of the  $\gamma_2(x_a, x_s)$  function contains a cliff near  $x_s = -5.50$  where the  $H_2$  norm increases suddenly. Holding  $x_a = -8.5$  but moving  $x_s = -5.50$  to  $-5.75$ , the  $H_2$  norm  $\gamma_2$  increases from 3.87 to 138. This occurs because the shift in the sensor location causes a small zero of the  $\mathbf{u}$ -to- $\mathbf{y}$  transfer function to move from the left-half-plane to the right-half-plane. When this occurs, the small right-half-plane zero introduces significant bandwidth limitations for disturbance rejection. A sensitivity function analysis indicates considerably inferior disturbance rejection at frequencies  $\omega < 10$ .

This non-robustness appears to indicate the importance of placing the sensor firmly within the region of high amplification, lest estimator errors grow beyond acceptable limits. For instance, in an actual two- or three-dimensional flow setup without *a priori*

knowledge of the optimal sensor placement, an experimenter could guess a sensor placement where amplification is expected. (Recall that the dynamics of fluid systems are often strongly non-normal (Chomaz 2005), so regions of transient amplification may not correspond well with unstable eigenmodes of the linearised dynamics.)

Besides these two major differences, the general form of the  $\gamma_2$  solution is similar to the case where disturbances are present everywhere. Level sets of  $\gamma_2$  have a near-triangular form, with penalties on placing the actuator too far downstream, placing the sensor too far upstream, and introducing excessive separation between sensors and actuators. The general similarities between figures 2(a) and 3(a) indicate that it is possible to find an actuator and sensor placement that is effective for both disturbance types. For example, if  $x_a = -3.50$  and  $x_s = 0.00$ , then  $\gamma_2 = 53.6$  when disturbances are present everywhere and  $\gamma_2 = 5.90$  when disturbances are concentrated upstream. These are acceptably close to the respective optimal values of 46.1 and 3.86. If other disturbance types retain the same qualitative nature of  $\gamma_2(x_a, x_s)$ , then a “universally” optimal placement could feasibly be sought.

We also perform brute force sampling for the two-actuator, two-sensor configuration with disturbances present everywhere. The placement is optimal at about  $x_a = -3.75, 2.75$  and  $x_s = -2.75, 3.75$ , for which  $\gamma_2 = 34.0$ . (Results are not plotted here.) As in the SISO case, these numbers are not precise, and are later refined using an iterative procedure. One common feature in MIMO results is that if one actuator or sensor is placed near the optimal position, then the effect of the other actuator or sensor placement on  $\gamma_2$  is generally not large.

#### 4.2. Conjugate gradient minimisation

The optimal placement for different numbers of actuators and sensors, as found using conjugate gradient minimisation, is shown in figure 4(a) for disturbances present everywhere. The iterative method more accurately puts the optimal SISO placement at  $x_a = -1.03$ ,  $x_s = 0.98$  and the optimal two-actuator, two-sensor placement at  $x_a = -3.78, 2.71$ ,  $x_s = -2.75, 3.74$ . An approximate symmetry around  $x = 0$  between actuator and sensor placement is apparent. Additionally, a simple pattern exists for configurations with an equal number of actuators and sensors. The optimal placement favors near-collocation of actuator and sensor pairs, with each actuator placed slightly upstream of each sensor. This allows the sensors to measure the effect of the actuators without a large time lag. As the number of actuators and sensors increases, the actuator-sensor pairs spread out across the spatial domain, and the spacing within pairs becomes tighter. Figure 4(a) shows that the placement of the pairs forms an orderly geometric pattern as the number of pairs increases.

A transfer function analysis of the controller gain  $K$  from  $\mathbf{y}$  to  $\mathbf{u}$  shows that the communication between sensors and actuators primarily occurs within pairs, especially at higher frequencies. (See (3.10) for the formulation of  $K$ .) This is illustrated in figure 5, which supposes the optimally-placed five-input, five-output system shown in the top row of figure 4(a). These three plots show the LQG gain from each sensor to each actuator, given that each sensor receives a signal  $\exp(i\omega t)$ . At lower frequencies (figure 5a), the gain from downstream sensors to upstream actuators is still nontrivial. This feedback aids the performance of the upstream actuators. At higher frequencies, the primarily diagonal structure of the gain matrices indicates that communication outside the pairs is weak. The diffusive nature of the Ginzburg–Landau operator dampens high frequency oscillations, so such oscillations do not propagate effectively across large distances. Therefore, high-frequency control is most effective within actuator-sensor pairs.

The optimal placements in the case of upstream disturbances is illustrated in Fig-

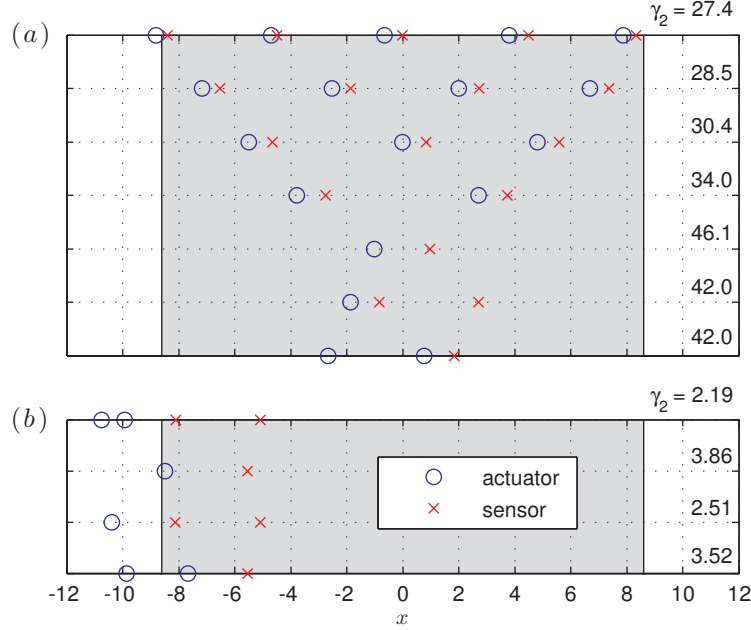


FIGURE 4. Optimal placement for different numbers of actuators and sensors. The  $H_2$  norm  $\gamma_2$  is tabulated for each configuration, and the region of amplification is shaded grey. (a): Disturbances present everywhere. (b): Disturbances introduced at  $x_d = -11.0$ .

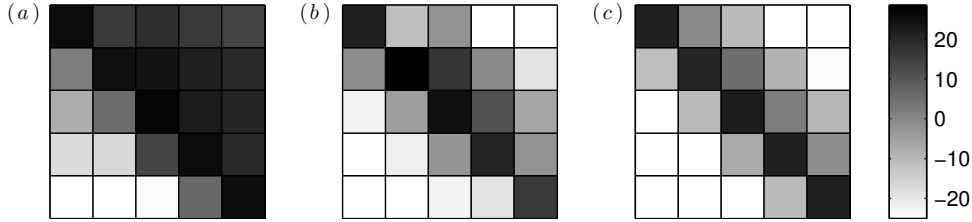


FIGURE 5. The LQG gain in the optimally-placed five-input, five-output system, shown in decibels. The block in row  $j$  and column  $k$  shows the gain from a signal  $\exp(i\omega t)$  in sensor  $k$  to actuator  $j$ , assuming that the sensors and actuators are ordered from upstream to downstream. (a): At  $\omega = 10^{-1}$ ; (b): at  $\omega = 10^1$ ; (c): at  $\omega = 10^3$ .

ure 4(b). For the limited number of configurations tested, the optimal actuator and sensor placements are upstream of the origin. Furthermore, the optimal sensor placement appears to be largely independent of the number of actuators. No other patterns are immediately obvious.

For each actuator-sensor configuration, figure 4 also tabulates the  $H_2$  norm  $\gamma_2$  from the disturbances to the perturbation and input costs. As expected,  $\gamma_2$  decreases as the number of actuators and sensors increases. This simply indicates that the control objective is easier to attain when more actuators and sensors are available. In figure 4(a), however, the decrease in  $\gamma_2$  tapers off when increasing the number of actuator-sensor pairs from one to five. Furthermore, in figure 4(b), the improvement to the base SISO case by adding one actuator is not as great as the improvement by adding one sensor. In choosing the number of actuators and sensors to use, an experimenter should consider a tradeoff between how much the perturbation and input need to be minimised, and how many actuators and

sensors can be afforded. Other factors, such as the way disturbances are introduced, also affect this decision. We may observe, for instance, that the multiplicative reduction in  $\gamma_2$  from SISO to two-input, two-output control is more significant in figure 4(b) than in figure 4(a).

#### 4.3. Further remarks

When performing an iterative technique, it is important to note the computational effort required. The linearised Ginzburg–Landau system presented here is accurately represented using only 100 states; however, iterating on higher-dimensional systems may be intractable if a large number of function calls is required. A complete discussion on the computational effort required to minimise  $\Gamma_2$  is beyond the scope of this paper. The effort would heavily depend on the choice of a minimisation algorithm, its numerical tolerances, and the initial conditions chosen.

As previously mentioned, each evaluation of  $\Gamma_2$  requires solving two  $N$ -by- $N$  Riccati equations (3.9), and each evaluation of  $\nabla\Gamma_2$  requires solving  $m_a + m_s$   $N$ -by- $N$  Lyapunov equations (3.16, 3.18). The bracketing function additionally requires a number of  $N$ -by- $N$  Riccati solutions that is generally not known *a priori*. With the algorithms chosen, scaling experiments show that for  $40 \leq N \leq 200$ , the CPU times of one Riccati solution and one Lyapunov equation solution both scale by about  $N^{2.5}$ . The CPU time of the former is about 2.7 times that of the latter. On a 2.66 GHz dual-core Intel Arrandale processor, each Riccati solution requires about 0.25 seconds for  $N = 100$ , and each Lyapunov equation requires about 0.10 seconds. The total number of equations to be solved depends heavily on the  $\gamma_2(\{x_a\}, \{x_s\})$  topology and the choice of tolerances and initial conditions. It suffices to state that the CPU time for convergence increases significantly as the number of actuators and sensors increases.

For the results presented in this study, the  $\gamma_2(\{x_a\}, \{x_s\})$  function topology is relatively simple. Global minima can be found by guessing multiple initial conditions and checking for common convergence. Beyond these simple configurations, however, convergence to a global minimum can be difficult. This is especially true when disturbances are only introduced upstream, or when unequal numbers of actuators and sensors are used. Good initial conditions are particularly important in these cases. Bad initial conditions may cause the iterator to converge very slowly, quit prematurely, or fail to converge to the global minimum. A global minimisation technique such as simulated annealing would then be necessary to ensure that a local minimum found is indeed the absolute minimum.

The choice of cost matrices also affects the computed optimal placement. As aforementioned, the vector costs used are  $\mathbf{J}_1 = \mathbf{Q}^{\frac{1}{2}}\mathbf{q}$  and  $\mathbf{J}_2 = \mathbf{R}^{\frac{1}{2}}\mathbf{u}$ , where  $\mathbf{Q}^{\frac{1}{2}} = \beta\mathbf{M}^{\frac{1}{2}}$  and  $\mathbf{R}^{\frac{1}{2}} = \mathbf{I}$ . The positive scalar  $\beta$  controls the balance between minimising  $\mathbf{q}$  and minimising  $\mathbf{u}$ . To quantify their sizes individually, let  $\gamma_q$  be the  $H_2$  norm of the transfer function from  $\mathbf{w}$  to  $\mathbf{J}_1$ , and let  $\gamma_u$  be the  $H_2$  norm of the transfer function from  $\mathbf{w}$  to  $\mathbf{J}_2$ . These are calculated using the LFT formulation (3.11) by respectively setting  $\mathbf{Z}_C = [\mathbf{C}_1 \ 0]$  and  $\mathbf{Z}_C = [0 \ -\mathbf{D}_{12}\mathbf{F}]$ , and computing  $\sqrt{\Gamma_2}$  by (3.12–3.13). It can be shown that  $\gamma_q^2 + \gamma_u^2 = \gamma_2^2$ . A measure of the perturbation size is then given by  $\gamma_q/\beta$ , and the input size by  $\gamma_u$ . For different choices of  $\beta$ , optimal positions and corresponding values of  $\gamma_q/\beta$  and  $\gamma_u$  are listed in table 2. (Note that the optimal controller and positions depend not on  $\mathbf{Q}$  and  $\mathbf{R}$  individually, but rather only  $\beta$ .)

We immediately see that within a fairly large range of  $\beta$ , the exact choice of  $\beta$  has little measurable impact on the optimal actuator and sensor placement. This indicates a robustness in the optimal placement to the precise choice of cost matrices, for sufficiently high  $\beta$ . As expected, a larger  $\beta$  is more effective at reducing the perturbation magnitude, but at a greater input expense. In practice, one would choose  $\beta$  based on this tradeoff. We

$\beta$	SISO				two-actuator, two-sensor					
	$x_a$	$x_s$	$ \gamma_q/\beta$	$\gamma_u$	$x_a$	$x_s$	$ \gamma_q/\beta$	$\gamma_u$		
1	-1.39	0.04	7.14	4.15	-3.25	3.17	-2.77	2.86	5.23	3.24
3	-1.02	0.92	6.59	6.33	-3.72	2.57	-2.79	3.65	4.86	4.69
7	-1.03	0.98	6.48	8.22	-3.78	2.71	-2.75	3.74	4.77	6.20
15	-1.04	1.01	6.44	11.1	-3.79	2.70	-2.73	3.77	4.74	8.30
50	-1.04	1.03	6.42	19.0	-3.80	2.70	-2.71	3.79	4.72	14.3

TABLE 2. Optimal placement, perturbation size, and input size for different  $\beta$ , with disturbances present everywhere.

select  $\beta = 7$  because it maintains a small perturbation magnitude using reasonably-sized inputs.

We also remark briefly that the controller designed from the linearised model is effective in the full, nonlinear Ginzburg–Landau model. The cubic term in (2.1) always drives the state  $q$  towards zero, aiding the controller in doing the same. Brief numerical experiments show, however, that the optimal placement in the nonlinear model does not necessarily correspond with that of the linear model. Further study is necessary to establish optimal placement in that case.

### 5. Comparison with previous approaches

We might naively believe that the optimal actuator and sensor placement could be determined directly from a global mode analysis. In this analysis, we would place sensors where the most unstable eigenmodes are large, so that growing disturbances would register a large output. Similarly, we would place actuators where the most unstable adjoint eigenmodes are large. This is supported by the fact that the construction of the LQG controller requires plant detectability and stabilisability (Doyle *et al.* 1989). Bagheri *et al.* (2009) and Åkervik *et al.* (2007) used this approach for actuator and sensor placement. While this method is plausible on intuitive grounds, it does not produce optimal results. With global and adjoint modes given by equation (2.3), we find for  $\mu_0 = 1.03\mu_c$  that there is one unstable mode and one unstable adjoint mode (Bagheri *et al.* 2009). These two mode magnitudes are bell curves, with peaks respectively at  $x = 7.28$  and  $x = -7.28$  (see figure 6a). If flow disturbances were introduced everywhere, and a sensor and actuator were placed at these two points, then (3.14) would yield  $\gamma_2 = 259$ . This is far from the optimal  $\gamma_2 = 46.1$  achieved by placing the actuator at  $x_a = -1.03$  and the sensor at  $x_s = 0.98$ .

The global mode analysis fails to reveal the optimal placement because the linearised Ginzburg–Landau operator is strongly non-normal. In general, the non-normality prevents global mode analysis from accurately predicting transient growth (Bagheri *et al.* 2009). In this system, as in Navier–Stokes systems, the disturbances that cause large transient growth are known not to correspond well with the most unstable eigenmodes (Trefethen *et al.* 1993). In principle, one may be able to circumvent this issue in a stable system by placing an actuator where an optimal harmonic forcing causes the greatest steady-state solution. The optimal harmonic forcing in the adjoint system could also yield a sensor placement. Bagheri *et al.* (2009) performed a related analysis in which the initial condition leading to the largest transient growth was sought. The magnitude of

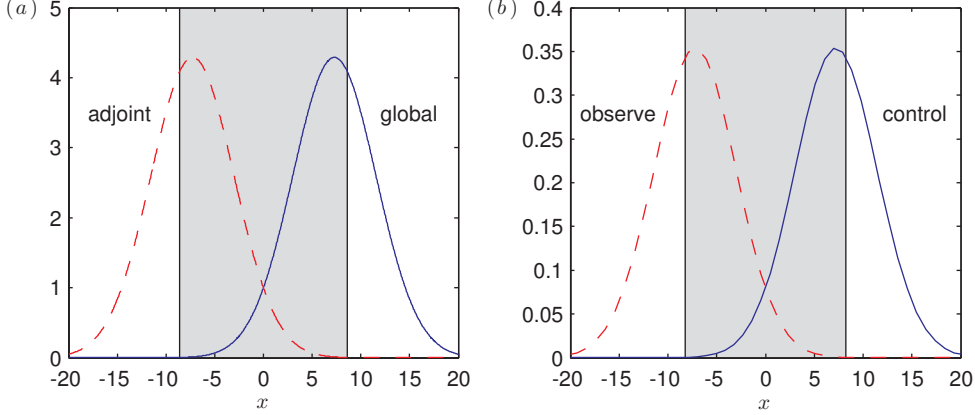


FIGURE 6. (a): Leading global and adjoint eigenmode magnitudes, for  $\mu_0 = 1.03\mu_c$ . (b): Leading modes of the observability and controllability Gramians (assuming full sensing and actuation), for  $\mu_0 = 0.96\mu_c$ . The region of amplification is shaded grey.

this optimal initial condition was a bell curve centred near the upstream boundary of the amplification region, and therefore would not yield the optimal actuator location. Consult Trefethen *et al.* (1993) and Schmid & Henningson (2000) for more details.

A similar analysis could be done using controllability and observability Gramians of the uncontrolled system with full sensing and actuation. This system is governed by  $(A, B, C)$  representing

$$\dot{\mathbf{q}} = A\mathbf{q} + B\mathbf{d} \quad (5.1a)$$

$$\mathbf{y} = C\mathbf{q}, \quad (5.1b)$$

where  $B = I$  and  $C = M$ . The adjoint system is governed by  $(A^+, C^+, B^+)$ . Because of the uneven grid spacing, the adjoint is not the same as the complex conjugate (Bagheri *et al.* 2009); specifically,

$$A^+ = M^{-1}A^*M \quad (5.2a)$$

$$B^+ = B^*M \quad (5.2b)$$

$$C^+ = M^{-1}C^*. \quad (5.2c)$$

The controllability Gramian  $W_c$  and the observability Gramian  $W_o$  are the solutions to the Lyapunov equations

$$AW_c + W_cA^+ + BB^+ = 0 \quad (5.3a)$$

$$A^+W_o + W_oA + C^+C = 0. \quad (5.3b)$$

In this analysis, we expect the leading eigenvector of  $W_c$  to be large where the state is sensitive to the disturbance  $\mathbf{d}$ ; this would appear to be a good place to put a sensor. Similarly, we expect the leading eigenvector of  $W_o$  to be large where the uncontrolled dynamics are most sensitive to disturbances; this would appear to be a good place to put an actuator. These eigenvectors are shown in figure 6(b) with  $\mu_0 = 0.96\mu_c$ , since Gramians are only well-defined for globally stable systems.

Once again, we find that this analysis does not correctly predict the optimal SISO placement. For this subcritical Ginzburg–Landau system, the optimal placement is  $x_a = -0.98$  and  $x_s = 0.95$ , yielding  $\gamma_2 = 42.8$ . The Gramian analysis, on the other hand, predicts  $x_a = -7.0$  and  $x_s = 7.0$ , yielding  $\gamma_2 = 188$ . This analysis fails because Gramians,

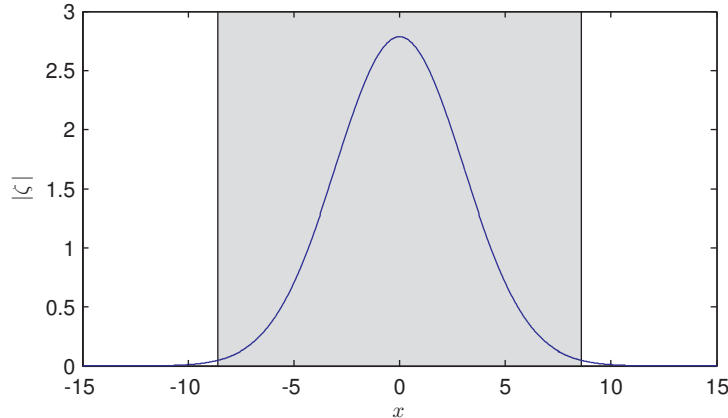


FIGURE 7. The global and adjoint mode overlap  $|\zeta(x)|$  for the unstable mode. The region of amplification is shaded grey.

by construction, decouple actuation from sensing. This is apparent from (5.3). When actuation and sensing are decoupled, the convective nature of information propagation is completely ignored. Placing the sensor so far downstream of the actuator effectively introduces a large time lag in the feedback control.

A method proposed by Giannetti & Luchini (2007) yields a better estimate of the optimal actuator and sensor placement when disturbances are present everywhere. Giannetti & Luchini define the “wavemaker” region as the part of the domain where

$$\zeta(x) = \frac{\phi_0(x) \bar{\psi}_0(x)}{\langle \phi_0, \psi_0 \rangle} \tag{5.4}$$

has a large magnitude, given a global mode  $\phi_0$  and adjoint mode  $\psi_0$ ; see (2.3). They employed a perturbation technique to show that in this wavemaker region, a change in  $A$  creates the largest possible change in the corresponding eigenvalue  $\lambda_n$ . Although we do not seek to change  $A$ , the wavemaker region nevertheless indicates a region of high dynamical sensitivity (Chomaz 2005). In such a region, an actuator has a powerful influence on the flow, and localised feedback is effective. Lauga & Bewley (2004) used the wavemaker to determine their actuator and sensor placement, and reported effective  $H_\infty$  control.

As shown in figure 7, the unstable global mode has the largest overlap with its corresponding adjoint mode at  $x = 0$  when  $\mu_0 = 1.03\mu_c$ . Therefore, we propose that placing actuators and sensors near the origin is a sensible initial condition for iterative function minimisation. Although this is a crude approximation for optimal placement, it remains more accurate than global mode and Gramian analyses.

## 6. Conclusion

The linearised Ginzburg–Landau equation is a simple model describing the temporal and spatial evolution of small flow perturbations. In this paper, we control the linearised Ginzburg–Landau equation by establishing a standard LTI state space with some number of actuators and sensors. We perform a perturbation analysis on the continuous algebraic Riccati equations that determine the  $H_2$  optimal controller. From this, we derive a formulation for the gradient of the controlled system’s  $H_2$  squared norm. This formulation, which is similar to but more efficient than the formulation of Hiramoto *et al.* (2000),

is applicable to any LQG-controlled system where actuation and sensing matrices are to be optimised. We use conjugate gradient function minimisation to iterate toward the linearised Ginzburg–Landau system’s optimal actuator and sensor placement. This is but one example of how the perturbation theory can be used.

The conjugate gradient results agree with brute force mappings of the  $H_2$  norm over a large domain. When one actuator and sensor are available, and flow disturbances are introduced everywhere, the optimal placement is  $x_a = -1.03$  and  $x_s = 0.98$  for the LQG cost matrices chosen. The brute force mappings show that there exist penalties for placing the actuator too far downstream, the sensor too far upstream, or the actuator too far upstream of the sensor. When an equal number of actuators and sensors is employed, the optimal placement is such that actuators and sensors are positioned in distinct pairs. Each actuator is slightly upstream of the corresponding sensor, and pairs are distributed throughout the region of amplification. We show that the optimal placement is relatively robust to the precise scaling of cost matrices.

When the disturbance is centred at  $x_d = -11.0$ , the optimal placement is  $x_a = -8.48$  and  $x_s = -5.55$ . Optimal MIMO placements are upstream of the origin, but no clear pattern emerges. Regardless of the way disturbances are introduced, the control system’s performance increases by adding more actuators and sensors, but the increase may not be significant. When optimising the control performance in an experimental setup, for instance, a greater improvement may be achieved by tuning the existing actuator and sensor placements than by simply adding more actuators and sensors.

The process of finding the optimal placement in the linearised Ginzburg–Landau system is completely tractable on a modern computer. Convergence to the global optimum can be difficult, however, when an unequal number of actuators and sensors is used, or when the flow disturbances are only introduced upstream.

Although global mode and Gramian analyses are standard techniques in LTI systems, neither is able to reproduce the optimal actuator and sensor placement. Both roughly suggest  $x_a = -7$  and  $x_s = 7$ , yielding an  $H_2$  norm four to six times larger than the true minimum when disturbances are present everywhere. The global mode analysis fails because the underlying dynamics are strongly non-normal, and the Gramian analysis fails because it inherently decouples actuation from sensing. On the other hand, we propose that wavemaker analysis is a better way to seek the optimal placement. Although it does not immediately yield the optimal placement, it provides a sensible guess of  $x_a = x_s = 0.0$ . This is a good initial condition for iterative minimisation.

The methods and results presented may be extended to two- or three-dimensional flow control problems. In such cases, the state size would likely be so large that Riccati and Lyapunov solutions would be computationally intractable. Therefore, each evaluation of the  $H_2$  norm and its gradient would likely require the construction of a reduced-order model, for instance using balanced proper orthogonal decomposition or the eigensystem realisation algorithm (Ma *et al.* 2010). Alternatively, iterative methods that bypass the model reduction process may be preferred (Luchini & Bewley 2010). Potentially faster minimisation algorithms, such as quasi-Newton iteration, may also be substituted (Press *et al.* 2007). We posit that with such techniques, optimisation of actuator and sensor placement in Navier–Stokes systems should remain computationally tractable using high-performance computing.

This work was supported by the National Science Foundation, grant CMMI-0932928, and K. C. received support from the United States Department of Defense (DoD) through the National Defense Science & Engineering Graduate (NDSEG) Fellowship Program.

We thank Prof. Tim Colonius, Prof. Paolo Luchini, Shervin Bagheri, and Miloš Ilak for guidance and advising.

## REFERENCES

- ÅKERVIK, E., HÖPFFNER, J., EHRENSTEIN, U. & HENNINGSON, D. S. 2007 Optimal growth, model reduction and control in a separated boundary-layer flow using global eigenmodes. *J. Fluid Mech.* **579**, 305–314.
- BAGHERI, S., HENNINGSON, D. S., HÖPFFNER, J. & SCHMID, P. J. 2009 Input-output analysis and control design applied to a linear model of spatially developing flows. *Appl. Mech. Rev.* **62** (2).
- CHOMAZ, J.-M. 2005 Global instabilities in spatially developing flows: non-normality and non-linearity. *Annu. Rev. Fluid Mech.* **37**, 357–392.
- CHOMAZ, J.-M., HUERRE, P. & REDEKOPP, L. G. 1988 Bifurcations to local and global modes in spatially developing flows. *Phys. Rev. Lett.* **60** (1), 25–28.
- COHEN, K., SIEGEL, S., LUCHTENBURG, M., MCLAUGHLIN, T. & SEIFERT, A. 2004 Sensor placement for closed-loop flow control of a “D” shaped cylinder wake. *AIAA Paper* 2004-2523.
- COSSU, C. & CHOMAZ, J.-M. 1997 Global measures of local convective instabilities. *Phys. Rev. Lett.* **78** (23), 4387–4390.
- DOYLE, J. C., GLOVER, K., KHARGONEKAR, P. P. & FRANCIS, B. A. 1989 State-space solutions to standard  $H_2$  and  $H_\infty$  control problems. *IEEE Trans. Autom. Control* **34** (8), 831–847.
- GIANNETTI, F. & LUCHINI, P. 2007 Structural sensitivity of the first instability of the cylinder wake. *J. Fluid Mech.* **581**, 167–197.
- GILLIES, E. A. 2000 Multiple sensor control of vortex shedding. *AIAA Paper* 2000-1933.
- HALIM, D. & MOHEIMANI, S. O. R. 2003 An optimization approach to optimal placement of collocated piezoelectric actuators and sensors on a thin plate. *Mechatron.* **13** (1), 27–47.
- HIRAMOTO, K., DOKI, H. & OBINATA, G. 2000 Optimal sensor/actuator placement for active vibration control using explicit solution of algebraic Riccati equation. *J. Sound Vib.* **229** (5), 1057–1075.
- KONDOH, S., YATOMI, C. & INOUE, K. 1990 The positioning of sensors and actuators in the vibration control of flexible systems. *JSME Int. J., Series III* **33** (2), 145–152.
- LAUGA, E. & BEWLEY, T. R. 2004 Performance of a linear robust control strategy on a nonlinear model of spatially developing flows. *J. Fluid Mech.* **512**, 343–374.
- LUCHINI, P. & BEWLEY, T. R. 2010 Methods for the solution of very large flow-control problems that bypass open-loop model reduction. In *Sixty-third Annual Meeting of the APS Division of Fluid Dynamics*. American Physical Society, Long Beach, CA.
- MA, Z., AHUJA, S. & ROWLEY, C. W. 2010 Reduced-order models for control of fluids using the eigensystem realization algorithm. *Theor. Comput. Fluid Dyn.* pp. 1–15, DOI 10.1007/s00162-010-0184-8.
- MOHEIMANI, S. O. R. & RYALL, T. 1999 Considerations on placement of piezoceramic actuators that are used in structural vibration control. In *Proc. 38th Conference on Decision & Control*, pp. 1118–1123. IEEE.
- PRESS, W. H., TEUKOLSKY, S. A., VETTERLING, W. T. & FLANNERY, B. P. 2007 *Numerical Recipes*, 3rd edn., chap. 10. Cambridge University Press.
- ROUSSOPOULOS, K. 1993 Feedback control of vortex shedding at low Reynolds numbers. *J. Fluid Mech.* **248**, 267–296.
- ROUSSOPOULOS, K. & MONKEWITZ, P. A. 1996 Nonlinear modelling of vortex shedding control in cylinder wakes. *Physica D* **97** (1–3), 264–273.
- SCHMID, P. J. & HENNINGSON, D. S. 2000 *Stability and Transition in Shear Flows, Applied Mathematical Sciences*, vol. 142, chap. 4.4. Springer.
- SKOGESTAD, S. & POSTLETHWAITE, I. 2005 *Multivariable Feedback Control: Analysis and Design*, 2nd edn., chap. 9.3. John Wiley & Sons Ltd.
- SREENIVASAN, K. R., STRYKOWSKI, P. J. & OLINGER, D. J. 1987 Hopf bifurcation, Landau equation, and vortex shedding behind circular cylinders. In *Proc. Forum on Unsteady Flow Separation* (ed. K. N. Ghia), pp. 1–13. ASME.

- TREFETHEN, L. N., TREFETHEN, A. E., REDDY, S. C. & DRISCOLL, T. A. 1993 Hydrodynamic stability without eigenvalues. *Sci.* **261** (5121), 578–584.
- WEIDEMAN, J. A. C. & REDDY, S. C. 2000 A MATLAB differentiation matrix suite. *ACM Trans. Math. Softw.* **26** (4), 465–519.
- WILLIAMSON, C. H. K. 1996 Vortex dynamics in the cylinder wake. *Annu. Rev. Fluid Mech.* **28**, 477–539.